# VULNERABILITY RISK ASSESSMENT OF NON ENGINEERED HOUSES BASED ON DAMAGE DATA OF THE 2009 PADANG EARTHQUAKE 2009 IN PADANG CITY, INDONESIA

Rusnardi Rahmat Putra[1,2], JunjiKIYONO[3]and AikoFURUKAWA[4]

[1] Lecturer, Department of Civil Engineering, Padang State University, Indonesia.
[2] Researcher, Department of Urban Management, Environmental Studies, Kyoto University, Japan, rusnardi.rahmat@gmail.com
[3] Professor, Department of Urban Management, Environmental Studies, Kyoto University, Japan, kiyono@quake.kuciv.kyoto-u.ac.jp
[4] Associate Professor, Department of Urban Management, Environmental Studies, Kyoto University, Japan, furukawa.aiko.3w@kyoto-u.ac.jp

## Abstract

Several powerful earthquakes have struck Padang during recent years, one of the largest of which was an M 7.6 event that occurred on September 30, 2009 and caused more than 1000 casualties. Following the event, We conducted a 12-site microtremor array investigation to gain a representative determination of the soil condition of subsurface structures in Padang. From the dispersion curve of array observations, the central business district of Padang corresponds to relatively soft soil condition with $Vs_{30}$ less than 400 m/s. because only one accelerometer was exist, we simulated the 2009 Padang earthquake to obtain peak ground acceleration for all sites in Padang city. By considering the damage data of the 2009 Padang earthquake, we produced seismic risk vulnerability estimation of non-engineered houses for rock, medium and soft soil condition. We estimated the loss ratio based on the ground response, seismic hazard of Padang and the existing damaged to non-engineered structure houses due to Padang earthquake in 2009 data for several return periods of earthquake events.

Key words; soil profile, Padang earthquake, microtremor array, seismic vulnerability.

## 1. Introduction

The Indonesian archipelago is located at the boundary of three major tectonic plates, the Indo-Australian, Pacific, and Eurasian plates, stretching from Sumatra in the west to Papua in the east (**Fig.1**).Indonesia is at the collision point of these three crustal plate. The high

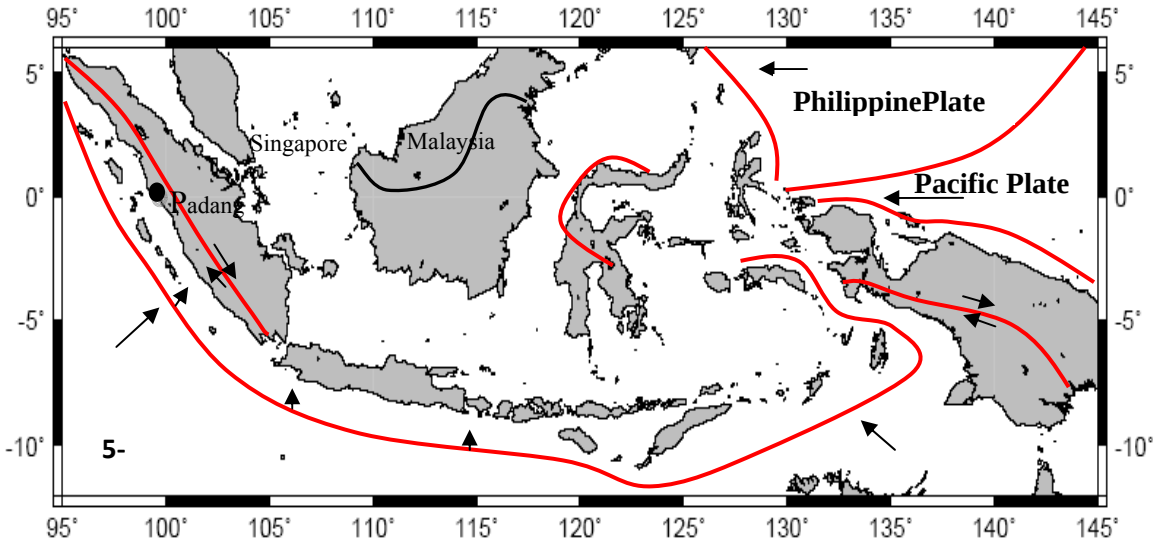


**Fig.1**Tectonic and plate boundaries, large arrows indicate the direction of plate motion. Black circle is Padang.

subduction-related seismicity in this region means that tsunami and other earthquake hazards are also high. Indonesia has approximately 17,504 islands, with a total land area of $1.92\times10^6$ km$^2$ and a sea area of $3.26\times10^6$ km$^2$. It has experienced a large number of earthquakes in the past. According to catalogued events, the number of earthquakes that have occurred in this region exceeds 48,000 with a magnitude greater than 4.0 from AD 1779 to 2010 (Rusnardi et al., 2010).

Most of the major historical earthquakes in Indonesia have caused significant damage to facilities (e.g., Utsu et al., 1992; Fauzi et al., 1999; EERI, 2010). Many large earthquakes have occurred in the shallow seas of the area that can produce massive tsunami like the 2004 Banda Aceh event. This earthquake off the coast of Sumatra resulted in hundreds of thousands of deaths and a million people homeless (Ahmed Ghobarah et al., 2006). The most recent one is the Mentawai tsunami that occurred on October 25, 2010.

The city of Padang ,located on the west coast of Sumatra in western Indonesia, lies close to the Sumatran subduction zone that is formed by the subduction of the Indo-Australian Plate beneath the Eurasian Plate. Relative motion of the plates occurs at a rate of about 50 to 70 mm/year and this is the main source of subduction-related seismicity in the area (Prawirodirjo et al., 2000). Based on our catalog, seven giant earthquakes have occurred in this region since records began: 1779 (Mw 8.4), 1833 (Mw 9.2), 1861 (Mw 8.3), 2004 (Mw 9.2), 2007 (Mw 7.9 and 8.4) and 2009 (Mw 7.6). The hypocenter of the Padang earthquake that occurred on September 30,2009was located in the ocean slab of the Indo-Australian Plate at -0.81°S, 99.65°E and at a depth of 80 km. It produced a high degree of shaking and the tremor was felt in the Indonesian capital, Jakarta, about 923 km from the epicenter. The tremors also were felt in neighboring countries such as Malaysia and Singapore (Laing, Aislinn, 2009). The earthquake caused landslides and collateral debris flows in the hills surrounding Lake Maninjau. A major landslide in Gunung NanTigo, Padang Pariaman completely destroyed some villages and forced road closures.

This 1900-km-long active strike-slip fault zone that runs along the backbone of Sumatra poses seismic and fault hazards to a dense population distributed on and around the fault zones (Natawidjaja et al., 2007). The Sumatran Fault is highly segmented. It consists of 20 major geometrically defined segments and the slip rate along the fault increase to the northwest, from about 5 mm/yr (Natawidjaja et al., 2007). This fault also has generated large destructive earthquakes, e.g., 1892 (Mw 7.1), 1943 (Mw 7.6) and 2007 (Mw 6.4). These faults are capable of generating strong ground motion in the future that would greatly affect vulnerable structures. According to our catalogs, the Sumatran Fault produces a very high annual rate of earthquakes, many of which occur in the shallow region under the island of Sumatra (**Fig.2**).

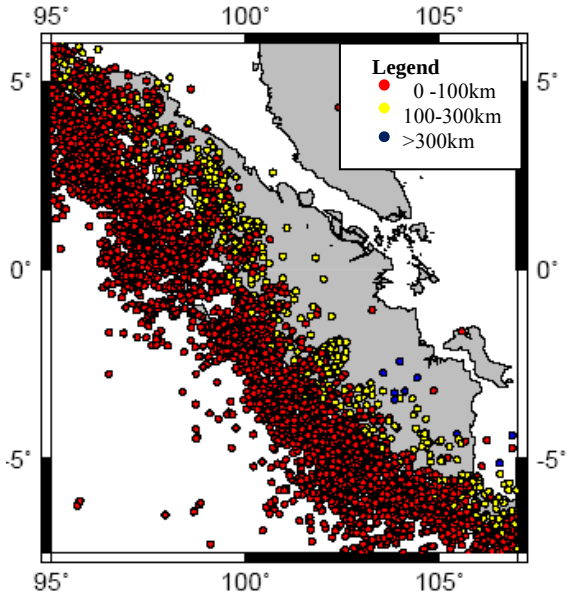


**Fig.2** Seismicity of Sumatra and western Indonesia, Mw>4 1779-2010

## 1.2 Regional Geology and Recent Earthquakes

The city of Padang , with a population of 856,814 people as of 2008, is the capital of West Sumatra province. The location of the city center is at 100.38°E, 0.95°S. The main part of Padang is situated on an alluvial plain between the Indian Ocean and the mountains. For the most part, the mountainous area is formed of Tertiary sedimentary rocks with outcrops of metamorphic rocks seen in some places. The alluvial plain spreads along the base of the mountains and is roughly 10 km wide in the east-west direction and 20 km wide in the north-south direction.

The topography of the Padang region (**Fig.3**) is very similar to the tsunami-damaged area of Miyagi Prefecture in Japan, that was inundated by as much as 4-5 km from the coast after the March 11, 2011 the off the Pacific Coast of Tohoku Earthquake (Mw 9.0). In Padang, about 600,000 people live in the coastal area (covering about 60 $km^2$). The population density is very high, about 8500 people/$km^2$. The city is located on the coast of the Indian Ocean between the Sumatran Fault and the Sunda Trench Fault. Both faults are active with slip rate ranging from

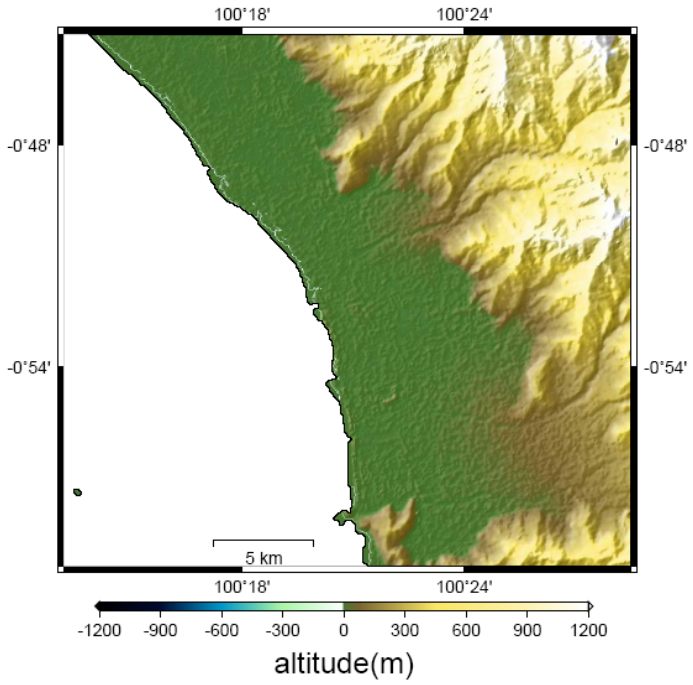


**Fig.3** Topography of Padang.

10 to 27 mm/year (Natawidjaja et al., 2007). According to our catalog, 2995 events with a magnitude greater than 4 occurred in this region from AD 1779 to 2010 (**Fig.5**). The seven giant earthquakes mentioned previously have all been strongly felt here. For example, the source of the 2009 Padang earthquake was located in the ocean slab of the Indo-Australian Plate.

It produced extensive shaking and severe damage to houses and buildings in Padang and Padang Pariaman, because its epicenter was about 60 km offshore from Padang (**Fig.4**). As the Padang earthquake was an intra-slab earthquake at intermediate depth with a comparable magnitude, the event did not generate a tsunami of significance (EERI, 2010).

Due to this earthquake, 1117 people were reported killed, 1214 severely injured, 1688 slightly injured, and 3 were left missing in West Sumatra. The earthquake also destroyed many houses, buildings and infrastructure (heavily damaged houses numbered 114,797, with 67,198 moderately damaged and 67,837 slightly damaged). In Padang, 5458 buildings sustained damage (Report, BNPB. 2009). This event occurred at the end of the working day, just 15 minutes after offices and schools closed; if it had struck earlier, the number of causalities would definitely have been higher as a result of building collapses.

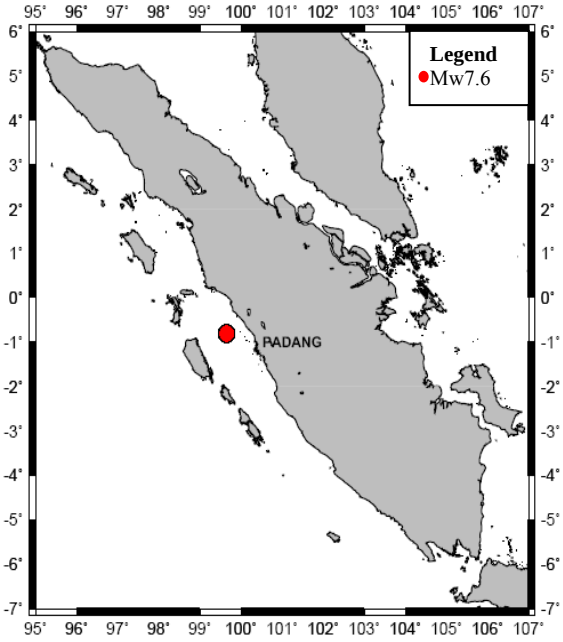


**Fig.4** Padang earthquake on September 30, 2009, Mw 7.6.

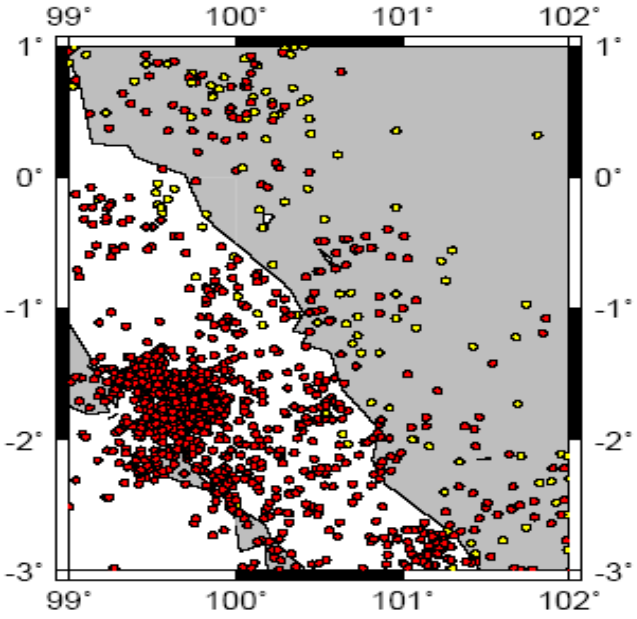


**Fig.5** Seismicity of Padang, Mw>4, from 1779- 2010.

There are four accelerometers in Padang. Three were donated by Engineers Without Borders Japan (EWBJ) and installed in 2008, and the other was installed by the Indonesian

Government's Bureau of Meteorology, Climatology and Geophysics (BMKG). However, only one ground motion record is available for the Padang earthquake. Due to an electric power cut during the earthquake, only the BMKG device recorded the time history of the earthquake. The observed record shows about 20 s of strong shaking with a peak ground acceleration (PGA) of 0.3 g and a predominant period of 0.5 s (**Fig.6**). The location of this station is a mountainous suburb about 12 km in from the coast. The subsurface condition at this station is rocky; the average shear wave velocity for the upper 30 m of the subsurface here, $V_{s30}$, is 697 m/s (Rusnardi et al., 2011).

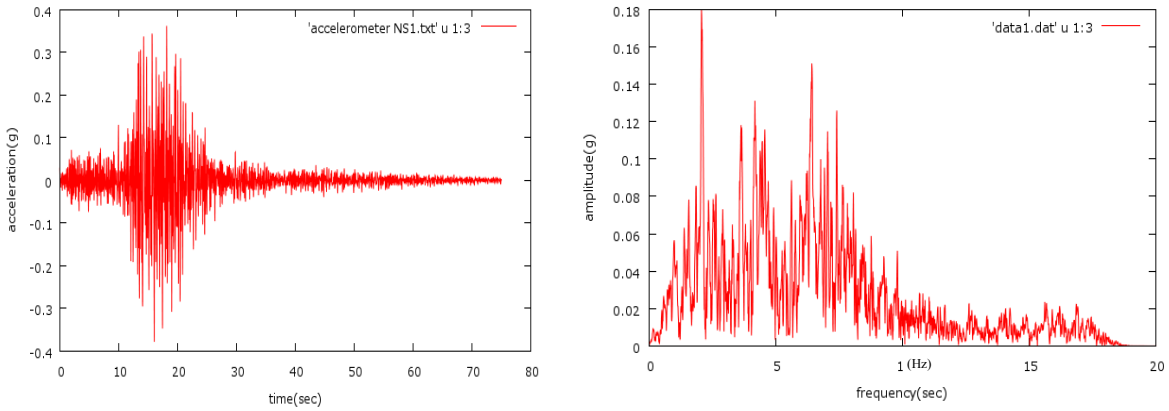


(a) (b)

**Fig.6** Accelerometer data for the 2009 Padang earthquake. (a) Time series of the Padang earthquake, (b) Fourier amplitude spectra.

### 1.3 Damage From the 2009 Padang Earthquake

The city of Padang covers an area of about 695 $km^2$ and is divided into 11 districts: B. T. Kabung, K. Tangah, Kuranji, L. Begalung, L. Kilangan, Nanggalo, P. Barat, P. Selatan, P.Timur, P. Utara, and Pauh (**Fig.7**). 51.0% of the land is forested, 28.52% is used for farming, 9.54% for housing and 7.1% for rice fields (Padang Local Government, 2009). The population of more than 857,000 is increasing by 2% per year. The K. Tangah district has the highest population and most extensive area compared with the other districts in the city. The population distribution and density is shown in **Table1 1 (**Padang Local Government, 2008).

The central business area of Padang is close to the coast and consist of several districts: P. Barat, P. Utara, P. Selatan and P. Timur, B.T. Kabung, K. Tangah (**Fig.7**). The downtown area

is utilized as a center of political and commercial activities. Although the Padang earthquake affected all districts of the city, the major damage occurred downtown, because about 80% of population lives near the coast (**Tables 2 and 3**).

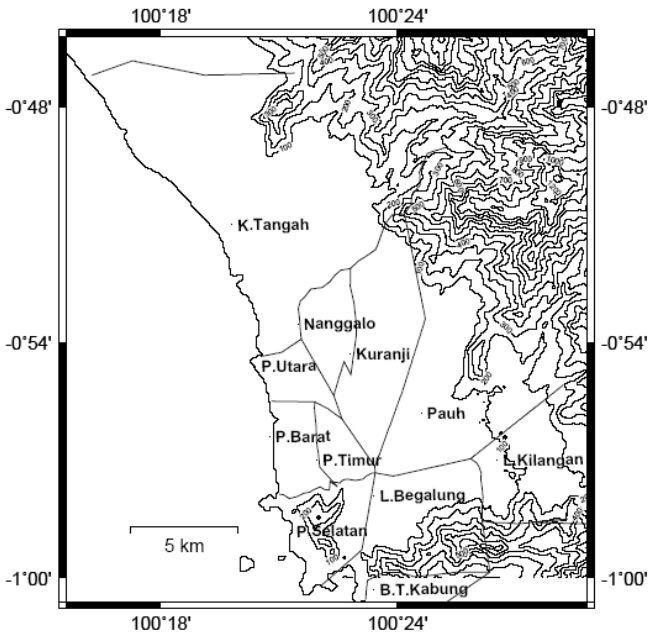


**Fig.7** The districts of Padang.

The majority of houses in the city are one- and two-storey non-engineered structures. These structures are typically built of confined masonry, with reinforced-concrete (RC) frames acting as confinement for the brick masonry walls. There are three general categories of houses in Padang: permanent houses (RC), semi-permanent houses (mix of RC and wood) and traditional houses (wood). Unfortunately, no detailed damage statistics are available for each type of building, so we cannot classify the category of the house. From **Table 2**, we estimated the house damage ratio for each district. We classified the damage ratio into severe, moderate and slight divisions. We found that the L. Kilangan district was the most severely damaged. Based on our survey of this district, we found mostly non-engineered houses.

This earthquake also affected lifelines in Padang. The strong ground shaking destroyed public water distribution pipes leading to 2,906 reported leakage points in total (Engineering report, local water supply agency, 2009). Damage to pipelines forced the cessation of water delivery to consumers for several weeks.

**Table1.**Population density of Padang city.

| Districts | Area ($Km^2$) | Population | Density |
|---|---|---|---|
| L. Kilangan | 86 | 43,531 | 506 |
| K. Tangah | 232.5 | 161,466 | 694 |
| L. Kuranji | 57.4 | 120,309 | 2096 |
| P. Barat | 7 | 61,437 | 8777 |
| P. Utara | 8.1 | 76,326 | 9446 |
| P. Selatan | 10 | 63,345 | 6316 |
| P. Timur | 8.2 | 87,174 | 10696 |
| Nanggalo | 8.1 | 58,801 | 7286 |
| L.Begalung | 30.9 | 106,641 | 3450 |
| Pauh | 146.3 | 53,669 | 367 |
| B.T. Kabung | 100.8 | 24,116 | 239 |
| Total | 695.2 | 856,815 | 4534 |

**Table2.** Damaged houses and buildings in each district (Padang local government, 2009)

| | Damaged houses | | | Total | Damage ratio | | | Damaged Building | | |
|---|---|---|---|---|---|---|---|---|---|---|
| District | Severe | Moderate | Slight | houses | Severe | Moderate+ | Slight+ | Severe | Moderate | Slight |
| L. Kilangan | 2441 | 2098 | 2315 | 9047 | 0.27 | 0.5 | 0.76 | 69 | 58 | 58 |
| K. Tangah | 7191 | 8423 | 7566 | 25888 | 0.28 | 0.6 | 0.9 | 246 | 176 | 170 |
| L. Kuranji | 4990 | 4749 | 4753 | 16098 | 0.31 | 0.6 | 0.9 | 133 | 144 | 170 |
| P. Barat | 2160 | 2202 | 2399 | 10604 | 0.2 | 0.41 | 0.64 | 372 | 152 | 163 |
| P. Utara | 2666 | 3036 | 3102 | 11446 | 0.23 | 0.5 | 0.77 | 201 | 125 | 81 |
| P. Selatan | 2436 | 2535 | 2887 | 8843 | 0.28 | 0.56 | 0.89 | 143 | 111 | 84 |
| P. Timur | 1670 | 3087 | 3395 | 12152 | 0.14 | 0.39 | 0.67 | 286 | 183 | 132 |
| Nanggalo | 2787 | 1911 | 1468 | 11528 | 0.24 | 0.41 | 0.53 | 190 | 79 | 73 |
| L. Begalung | 4976 | 5305 | 6506 | 17993 | 0.28 | 0.57 | 0.93 | 198 | 161 | 150 |
| Pauh | 1129 | 1426 | 2005 | 6947 | 0.16 | 0.37 | 0.66 | 63 | 118 | 62 |
| B.t. Kabung | 1151 | 1044 | 1219 | 3414 | 0.34 | 0.64 | 1 | 112 | 139 | 56 |
| Total | 33597 | 35446 | 37615 | | | | | 2013 | 1446 | 1199 |

**Table 3.**Damaged infrastructure for each district (Padang local government, 2009).

| | Damaged infrastructure | | | | | | | | |
|---|---|---|---|---|---|---|---|---|---|
| | Road | | | Bridges | | | Irrigation | | |
| District | Severe | Moderate | Slight | Severe | Moderate | Slight | Severe | Moderate | Slight |
| L. Kilangan | - | - | - | - | - | - | - | - | - |
| K. Tangah | 1 | 1 | - | 1 | 2 | - | 3 | - | - |
| L. Kuranji | 2 | 1 | - | 1 | 2 | - | 1 | - | - |
| P. Barat | 1 | 4 | - | 2 | 3 | - | - | - | - |
| P. Utara | 1 | 2 | - | - | 5 | - | - | - | - |
| P. Selatan | 1 | 4 | - | 1 | 2 | 1 | - | - | - |
| P. Timur | - | 3 | - | - | 1 | 1 | - | - | - |
| Nanggalo | 1 | 1 | - | - | 3 | - | - | - | - |
| L. Begalung | 1 | 2 | - | 2 | - | - | 1 | - | - |
| Pauh | - | 2 | - | - | - | 1 | 1 | - | - |
| B.t. Kabung | - | 2 | - | 1 | 1 | - | 1 | - | - |
| Total | 8 | 22 | 0 | 8 | 19 | 3 | 7 | 0 | 0 |

## 2. Site Characterization by Microtremor Observation

### 2.1 Microtremor array observations

The velocity of surface waves is well known to vary as a function of frequency (or period) due to dispersion. Since dispersion is a function of subsurface structure, the substructure can be estimated from a Rayleigh wave dispersion curve. We carried out microtremor array investigations using 12 sites at several districts in Padang (**Fig.10**). Dispersion curves were calculated using the SPAC method (Aki, 1957) to obtain a velocity structure from the microtremor recordings. An outline of the procedure follows. It is necessary to simultaneously record microtremors with an instrument array of at least three stations. The dispersion of a measured surface wave is a response to the subsurface structure directly below the array, and the estimation of the subsurface structure causing the dispersion is determined by means of inversion of Rayleigh waves. The basic principles of the SPAC method assume that the complex wave motions of microtremors are stochastic processes in time and space. A spatial autocorrelation coefficient for a circular array can then be defined when the waves composing the microtremor (i.e., the surface waves) are dispersive. Hence, the spatial autocorrelation is a function of phase velocity and frequency. Rayleigh wave records were measured for the 12-array observation sites

using the SPAC method and inversion analysis was undertaken on the observed dispersion curves (Figure 11) to estimate the soil profiles. In the inversion analysis, the Particle Swarm Optimization (PSO) algorithm was adopted to solve the non-linear optimization problem (Keneddy and Eberhart, 1995). The basic procedures of PSO are outlined below.

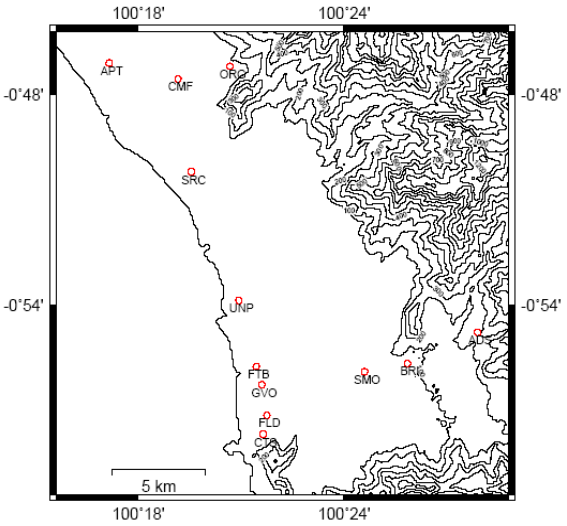


**Fig.10** Array observation sites

The particle swarm concept originated as a simulation of simplified social system. The original intent was to graphically simulate the choreography of bird of a bird block or fish school. However, it was found that particle swarm model can be used as an optimizer, PSO simulates the behaviors of bird flocking. Suppose the following scenario: a group of birds are randomly searching food in an area. There is only one piece of food in the area being searched. All the birds do not know where the food is. But they know how far the food is in each iteration. So what's the best strategy to find the food? The effective one is to follow the bird which is nearest to the food. PSO learned from the scenario and used it to solve the optimization problems. In PSO, each single solution is a "bird" in the search space. We call it "particle". All of particles have fitness values which are evaluated by the fitness function to be optimized, and have velocities which direct the flying of the particles. The particles fly through the problem space by following the current optimum particles. PSO is initialized with a group of random particles (solutions) and then searches for optima by updating generations. In every iteration, each particle is updated by following two "best" values. The first one is the best solution (fitness) it has achieved so far. (The fitness value is also stored.) This value is called pbest. Another "best" value that is tracked by the particle swarm optimizer is the best value, obtained so far by any

particle in the population. This best value is a global best and called gbest. When a particle takes part of the population as its topological neighbors, the best value is a local best and is called lbest.

We estimate the subsurface structure of the model by solving a nonlinear minimizationproblem with the fitness function below.

(1)

(2)

where is particle velocity of the component in dimension d in the interaction, is the particle position of the component in dimension d in interaction, and are constant weight factors, is the best position achieved by particle , is the best position found by the neighbor of particle , and are random factors in the [0,1] interval and is the inertia weight.Before performing the inversion analysis, the subsurface structure was assumed to consist of horizontal layers of elastic and homogeneous media above a semi-infinite elastic body. The shear wave velocity and thickness of each layer are the parameters determined by the inversion analysis. The results enable us to determine the condition of shallow subsurface structures (Ono et al., 2010). The outline of the SPAC method for the phase velocity calculation of Rayleigh waves follows.

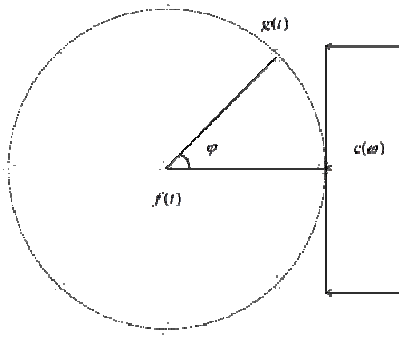


**Fig 11**.Microtemor array observation schema

(3)

$A_f(\omega)$, $A_g(\omega)$ and $\emptyset_f(\omega)$, are difference between the amplitude of $\emptyset_g(\omega), F(\omega), G(\omega)$ respectively. Futher cross correlation in the frequency region of the two waveforms will be as follows.

$$CC_{fg} = F(\omega) \cdot \overline{G(\omega)} = A_f(\omega) \cdot A_g(\omega) \cdot exp\big(i\Delta\emptyset(\omega)\big) \tag{5}$$

It shows the phase difference of$\Delta\emptyset(\omega)$

$$\Delta\emptyset(\omega) = \frac{\omega r}{c(\omega)} \tag{6}$$

$c(\omega)$ is the phase velocity from the phase difference.

$$CC_{fg} = A_f(\omega) \cdot A_g(\omega) \cdot exp\left(i\frac{\omega r}{c(\omega)}\right) \tag{7}$$

The complex coherence of two waveforms is defined by the following equation.

$$COH_{fg}(\omega) = \frac{CC_{fg}(\omega)}{A_f(\omega) \cdot A_g(\omega)} = ex\,p\left(i\frac{\omega r}{c(\omega)}\right) \tag{8}$$

$$Re\left(COH_{fg}(\omega)\right) = \cos\left(i\frac{\omega r}{c(\omega)}\right) \tag{9}$$

.

$$c(\omega, \varphi) = \frac{c(\omega)}{cos\varphi} \tag{10}$$

$$SPAC(\omega, r) = \frac{1}{2\pi}\int_0^{2\pi} exp\ (i\frac{\omega r}{c(\omega)}cos\varphi)d\varphi \tag{11}$$

$$Re\big(SPAC(\omega, r)\big) = \frac{1}{2\pi}\int_0^{2\pi} \cos(i\frac{\omega r}{c(\omega)}cos\varphi)d\varphi \tag{12}$$

$$J\left(\frac{\omega r}{c(\omega)}\right) = \frac{1}{2\pi}\int_0^{2\pi} exp(\frac{\omega r}{c(\omega)}cos\varphi)d\varphi \tag{13}$$

where $Jo(x)$ is the zero-order Bessel function of the first kind of x, and $c(\omega)$ is the phase velocity at frequency $\omega$. The SPAC coefficient $\rho(r,\omega)$ can be obtained in the frequency domain using the Fourier transform of the observed microtremors.

$$Re\big(SPAC(\omega,r)\big) = J\left(\frac{\omega r}{c(\omega)}\right) \tag{14}$$

From the SPAC coefficient$\rho(r,\omega)$, the phase velocity is calculated for every frequency from the Bessel function argument of equation. 15 and the velocity model can be inverted**.**

Layer thickness and the average S-wave velocity in Figure 6 each array site. For the average S wave velocity model obtained by averaging the estimated ground structure of the array site was to be calculated by a weighted average using a S-wave velocity structure is estimated as a weighted layer thickness.

$$\overline{V_s} = \sum V_{si} \cdot \frac{H_i}{H} \tag{15}$$

From the dispersion curve, we can produce an interpretation $Vs_{30}$ (average shear wave velocity for the upper 30 m) as show in **Table 4**. In **Fig.13 (b)** shows the contours of $Vs_{30}$ for every 200 m/s increment.

**Table 4.** Results of microtremor array observations (Vs, average shear wave velocity of the upper 30 m of the soil.)

| Site name | 1st layer Thickness (m) | 1st layer Vs (m/sec) | 2nd layer Thickness (m) | 2nd layer Vs (m/sec) | 3rd layer Thickness (m) | 3rd layer Vs (m/sec) | 4th layer Thickness (m) | 4th layer Vs (m/sec) | Average Vs(30) |
|---|---|---|---|---|---|---|---|---|---|
| ADS | 3 | 163 | 8 | 409 | ~ | 1891.3 | - | - | 693 |
| BRI | 7 | 344 | 13.8 | 526 | 38.9 | 744 | ~ | 1219 | 600 |
| SMO | 1.9 | 135 | 9.7 | 468 | 35.7 | 508 | ~ | 789.4 | 506 |
| GVO | 43.8 | 198 | 17.8 | 308 | 35.3 | 356.7 | ~ | 515.3 | 198 |
| FTB | 21 | 158 | 45 | 263 | 35.1 | 378.8 | ~ | 432.4 | 189 |
| UNP | 28.2 | 163.2 | 59.3 | 284 | ~ | 469 | - | - | 171 |
| CTS | 5.2 | 96.8 | 12.5 | 184 | 44.8 | 296.8 | ~ | 471.6 | 233 |
| FLD | 17.7 | 177 | 35.6 | 315 | 13 | 410.3 | ~ | 479.6 | 232 |
| ORG | 26.1 | 372.4 | 12.6 | 492 | ~ | 1266.3 | - | - | 388 |
| CMF | 5.7 | 163 | 30.7 | 197 | 77.2 | 293.6 | ~ | 423.8 | 190 |
| SRC | 30 | 190 | 40.2 | 257 | ~ | 290 | - | - | 190 |
| APT | 20.5 | 146.7 | 53.1 | 234 | 102 | 348.7 | ~ | 555.3 | 175 |

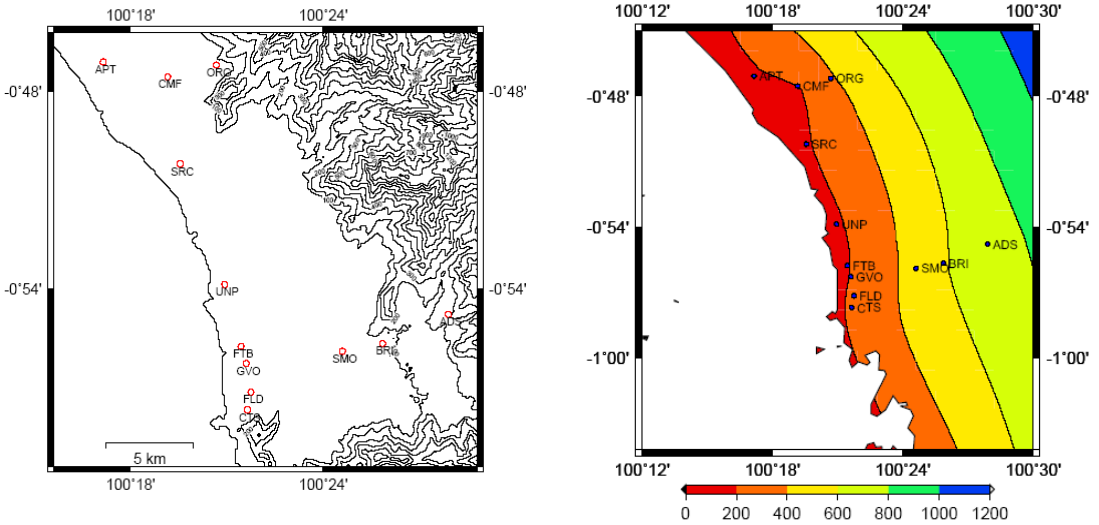


(a) (b)

**Fig.13** Observation sites and distribution of average shear wave velocity, (a) Array observation sites, (b) Contour of $V_{s30}$

## 3. Seismic Risk Assessment and Loss Estimation

Seismic risk assessment and loss estimation is an essential first step to seismic hazard reduction for a large structural inventory. Knowing the seismic risk and potential losses allows for proper budgetary planning, raising public awareness, assessment and allocation of the

necessary manpower for mitigation and disaster management operations, educating the public and professionals on preparedness and mitigation, and prioritization of retrofit applications (EERI, 1997). Components of seismic risk assessment and loss estimation are (1) Hazard analysis; (2) Local site effects (microzonation); (3) Exposure information (structural inventory); (4) Vulnerability analysis; (5) Estimation of risk and loss (Coburn, et al., 1994; CSSC, 1999; Chandler and Nelson, 2001; Bendimerad, 2001). These components are briefly described in the following subsections.

The vulnerability is the proneness of some category of element at risk to undergo adverse effects inflicted by potential earthquake.

Seismic risk probability = seismic hazard probability (occurrences probability vs. PGA)
x vulnerability loss (loss vs. PGA) (16)

### 3.1 Seismic Hazard Analysis For Padang City

This study falls primarily within the disciplines of geology and seismology with input from civil engineering. Probabilistic Seismic Hazard Analysis (PSHA) aims to quantify the uncertainties and produces an explicit description of the distribution of future shaking that may occur at a site (Baker, 2008). We consider all possible earthquake events and estimate ground motion along with their associated probabilities of occurrence in order to assess design ground motion for structure. The annual probability of exceedance is determined for some level of earthquake shaking at site. In this study, we consider the earthquakes of which magnitudes are larger than 4.0 in moment magnitude scale,and adopt an area model to determines source because earthquake events may occur anywhere in the region as showed in **Fig.5**. According to our catalog ,about 2,995 events occurred in this region during the period from 1779 to 2012 (**Fig.5**). Many giant earthquakes such as in 1779 (Mw8.4), 1833 (Mw9.2), 1861 (Mw 8.3), two times in 2007 (Mw7.9 and 8.4), the recent Padang earthquake on September 30, 2009 (Mw7.6) and the latest Mentawai earthquake on October 25, 2010 (Mw7.2) are included. The recent 2010 Mentawai earthquake produced tsunami.

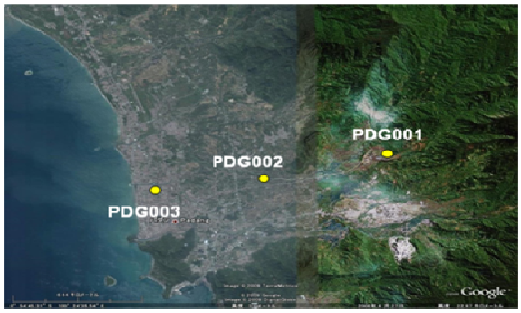


**Fig.14** Accelerometer stations at Padang city

We compared several existing attenuation equations and selected a suitable one for Indonesia. They are compared with ground motion attenuation observed at three stations **(Fig.14)**. From the comparison, we adopted Fukushima's attenuation as an appropriate equation and applied to seismic hazard analysis. In addition, we calculated the seismic hazard for peak ground acceleration PGA with 10% probabilities of exceedance in 50 years by using equation 17.

Seismic hazard curve describes the aggregate hazard at a particular site. The seismic hazard *H (A)* is defined as the annual occurrence rate of earthquake that produce a ground motion exceeding a given level at a specific site, based on Cornel et al. (1968). The overall hazard is composed of the respective contribution *Hi (A)* from each source zones, *i,* out of the set of zone I as shown in Eq. (17). The range of possible $M_i$ and $R_i$ have been discretized into $n_M$ and $n_R$ interval, respectively, by using the discretization technique.

$$\lambda(IM>x)=\sum_{i=1}^{sources}\lambda_m(M_i>m_{min})\sum_{j=1}^{n_M}\sum_{k=1}^{n_R}P\,(IM>x|m_j,r_k)\;*P(M_i=m_j)P(R_j=r_k) \qquad (17)$$

where $\lambda(IM>x)$ is the annual earthquake occurrence rate of which peak value exceeds a given level, $x$; $\lambda\ (M_i>m_{min})$ is the rate of earthquake with magnitude greater than $m$, $P(IM>x|m_j,r_k)$ is the probability of occurrence of the associated magnitude and distance; $P(M_i=m_j)$ is the probability associated with all magnitude between $m_j$ and $m_{j+1}$ to the discrete value $m_j$; $P(R_j=r_k)$ is the probability of occurrence of the associated distance.

One of the advantages of probabilistic seismic hazard analysis is that we can account for all possible earthquake source in area. A disadvantage of PSHA is that concept of design earthquake is lost. Which earthquake scenario is most likely to cause PGA>x?.

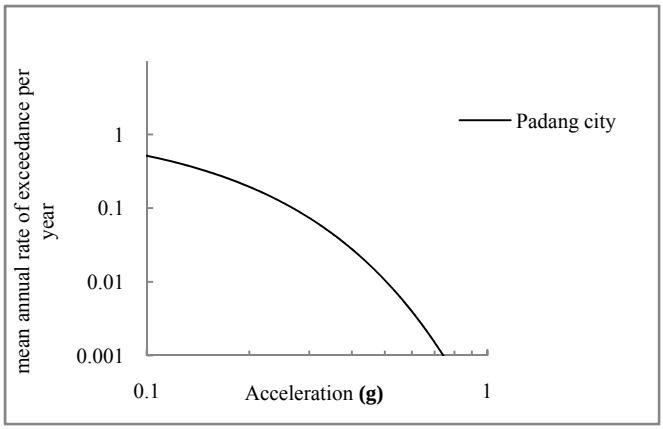


**Fig.20** Seismic hazard curve for Padang city at 10% probability of exceedance in 50 years.

### 3.2 Exposure Information

Exposure is the value of the structures and contents, business interruption, lives and other valuables that may lead to a potential loss in a seismic event. Depending on the scope of the risk assessment study, exposure may include a single building with its occupants and contents, or may include all constructed facilities in a region including all buildings with their occupants and contents, lifelines, and utility systems. Building exposure information for a region requires a standard systematic inventory system that classifies the structures according to their type, occupancy, and function so that realistic estimates of seismic risk and loss can be made. Such as an inventory data collection and classification system.

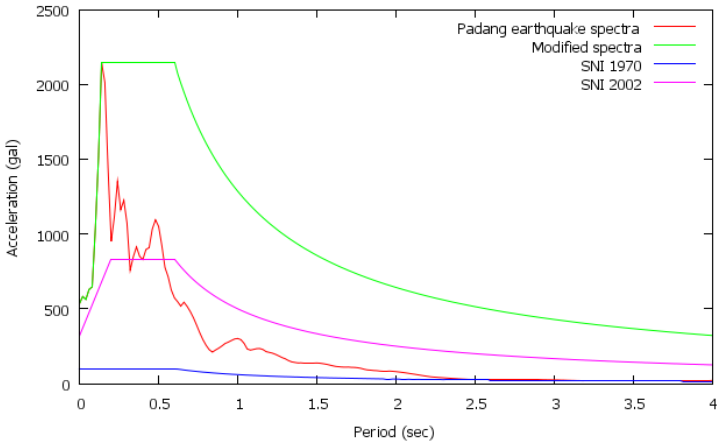


**Fig 5.2** Comparison response spectra between actual Padang earthquake and existing Indonesian code (SNI 2002) for rock site condition.

### 3.3 Ground Shaking Due to Padang Earthquake September 2009

The shaking level will shows that majority of the Padang city is indentified with a violent shaking severity rating in Padang city.

#### 3.3.1 Ground Response analyses

Several methods for evaluating the effect of local soil conditions on ground response during earthquake are presently available. Most of these methods are based on the assumption that main response in a soil deposit are caused by the upward propagation of shear waves from underlying rock formation. Analytical procedures based on this concept in cooperating non linear soil behavior, have been shown to give results in good agreement with field observation in a number of cases. Accordingly, they are finding increasing use in earthquake engineering for predicting response within soil deposit and the characteristics of ground surface.

There was no instrumentally observed record of the shaking in the downtown area of Padang during the earthquake or only one time series record is available in mountainous area. However, BMKG recorded the shaking by a strong-motion seismograph placed on a rocky site in Andalas University (BMKG), which it is about 11km eastern site from coastal (**Fig.15**).

As known, Engineer Without Border of Japan installed 3 accelerometer devices at 3 sites in Padang; Andalas University, sub-mayor office and government office, unfortunately these instruments did not record ground motion during earthquake caused of the electric was cutting off.

Caused of this reason, we simulated the 2009 Padang earthquake ground motion from Andalas University to target site in downtown of Padang city by using sub soil structure or soil profile from our microtermor array observation.

The input data, a time series of September 30$^{th}$ 2009, Padang earthquake was recorded at Andalas university (BMKG) in **Fig 15**. Accelerometer provided by meteorology and geophysics agency of Indonesia government. First step, ground motion at Andalas University was analyzed to get new ground motion at the bedrock, second step, ground motion at the bedrock simulated to the surface target site as **Fig.16**. Considered peak horizontal acceleration of the input is N-S direction.

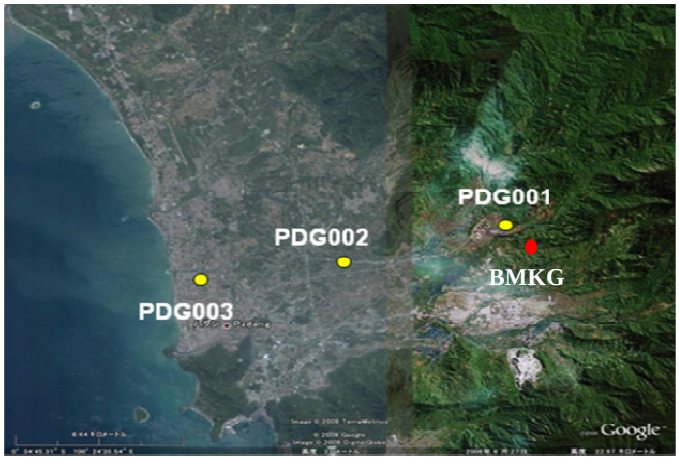


**Fig.15** Accelerometer devices in Padang, yellow circles are accelerometers provided by EWBJ and red circle is accelerometer provided by Indonesian Government.

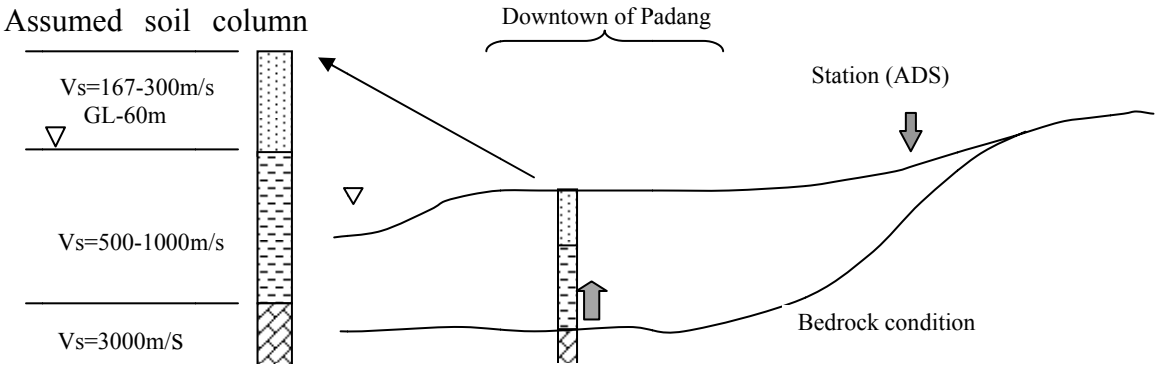


**Fig.16** Conceptual diagram of synthesizing process

From the ground response analysis, the ground motion at the surface for some sites and by using kriging method to interpolate the results, we obtained all ground motion in Padang city and plotted in **Fig.17.** The peak of ground motion is increasing from the rock site (high land) to downtown (soft soil condition) about 1.5 times higher.

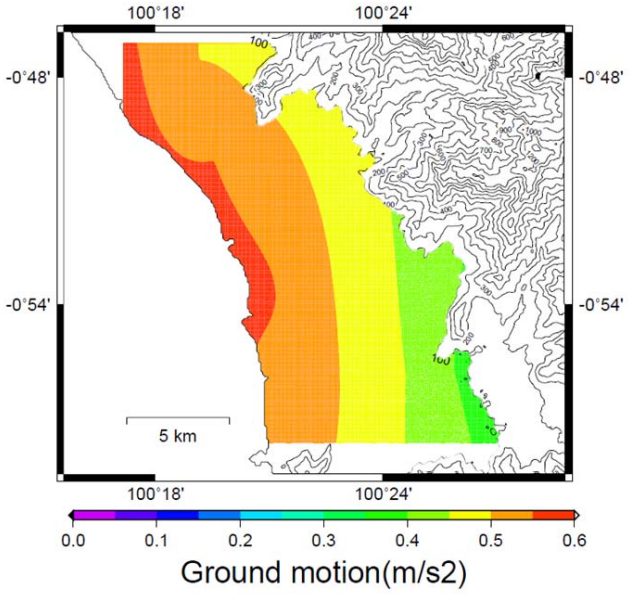


**Fig.17** Ground motion whole Padang city.

### 3.4 Vulnerability Assessment

Vulnerability can simply be defined as the sensitivity of the exposure to seismic hazard(s). The vulnerability of an element is usually expressed as a percentage loss (or as a value between zero and one) for a given hazard severity level (Coburn et al., 1994). In a large number of elements, like building stocks, vulnerability may be defined in terms of the damage potential to a class of similar structures subjected to a given seismic hazard.

Vulnerability analysis reveals the damageability of the structure(s) under varying intensity or magnitudes of ground motion. Multiple damage states are typically considered in the analysis. Based on the data of damaged houses by ground shaking of Padang earthquake in 2009 (**Table 1**). We estimated damage ratio for residential in Padang and based on the ground shaking at each area ((soft, stiff soil and rock). In figure 18 shows the soil characteristic is classified into 3 type based on its shear velocity, 0-150 m/s is soft, 151-300m/s is stiff soil and upper 300m/s is rock. The damage degree is classified into 3 categories, severe, moderate (+) and slight (+). Here, for each categorize means is; severity is from major structural damage to totally collapsed (un-repairable), moderate is widespread, extensive non-structural damage (repairable) and slight is non-structural damage (easy repairable). The ground shaking acceleration for each area is 0.56g, 0.45g and 0.36g for soft, stiff soil and rock respectively. The damage ratio (%) for each classified

soil is; soft is 25, 53, 80, medium is 22, 46, 71, rock is 19, 39, 60 for severe, moderate(+) and slight(+) respectively.

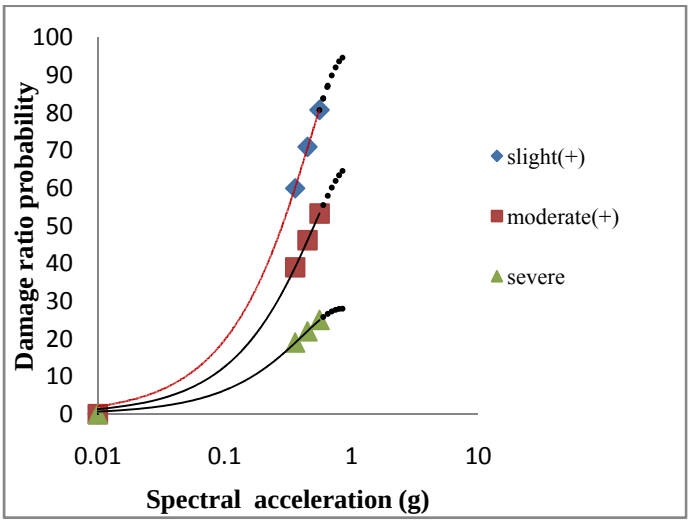


**Fig.18** Vulnerability functions (based on PGA) for low rise residential.

### 3.5 Seismic Risk Vulnerability

Risk combines the expected losses from all levels of hazard severity, also taking their occurrence probability into account, while vulnerability of an element is usually expressed for a given hazard severity level (Coburnet al. 1994). Loss is defined as the human and financial consequences of damage, including injuries or deaths, the costs of repair, or loss of revenue. In this paper consequences of damage and the cost of repair are taking account only. The distinction between risk and loss is often very loose and, based on their definition; these terms are sometimes used interchangeably. Since the standard definition of risk is a probability or likelihood of loss, between zero and one, it may be more appropriate to express risk.

**Table 3. Damaged houses estimation due to Padang earthquake 30 September 2009 (Padang local government, 2009)**

| | Damaged houses | | | Total | Damage ratio | | | Total damaged in US $ (Rp) |
|---|---|---|---|---|---|---|---|---|
| District | Severe | Moderate | Slight | houses | Severe | Moderate+ | Slight+ | |
| L. Kilangan | 2441 | 2098 | 2315 | 9047 | 0.27 | 0.5 | 0.76 | $363 million |
| K. Tangah | 7191 | 8423 | 7566 | 25888 | 0.28 | 0.6 | 0.9 | $1.21 billion |
| L. Kuranji | 4990 | 4749 | 4753 | 16098 | 0.31 | 0.6 | 0.9 | $767 million |
| P. Barat | 2160 | 2202 | 2399 | 10604 | 0.2 | 0.41 | 0.64 | $347 million |
| P. Utara | 2666 | 3036 | 3102 | 11446 | 0.23 | 0.5 | 0.77 | $450 million |
| P. Selatan | 2436 | 2535 | 2887 | 8843 | 0.28 | 0.56 | 0.89 | $399 million |
| P. Timur | 1670 | 3087 | 3395 | 12152 | 0.14 | 0.39 | 0.67 | $381 million |
| Nanggalo | 2787 | 1911 | 1468 | 11528 | 0.24 | 0.41 | 0.53 | $360 million |
| L. Begalung | 4976 | 5305 | 6506 | 17993 | 0.28 | 0.57 | 0.93 | $836 million |
| Pauh | 1129 | 1426 | 2005 | 6947 | 0.16 | 0.37 | 0.66 | $214 million |
| B.t. Kabung | 1151 | 1044 | 1219 | 3414 | 0.34 | 0.64 | 1 | $176 million |
| Total | 33597 | 35446 | 37615 | | | | | $5.5 billion |

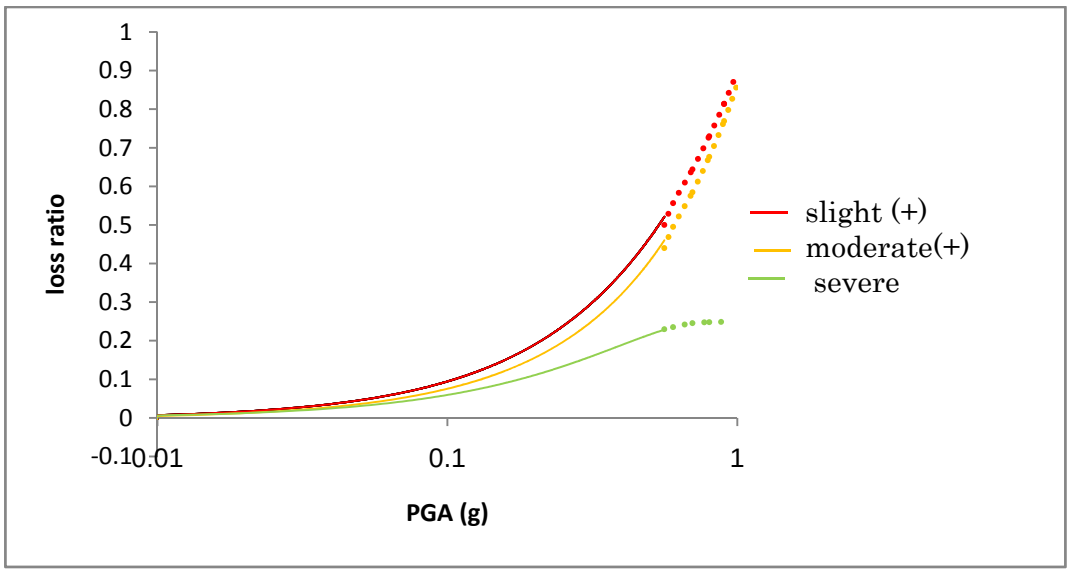


**Fig.19** Loss ratio prediction

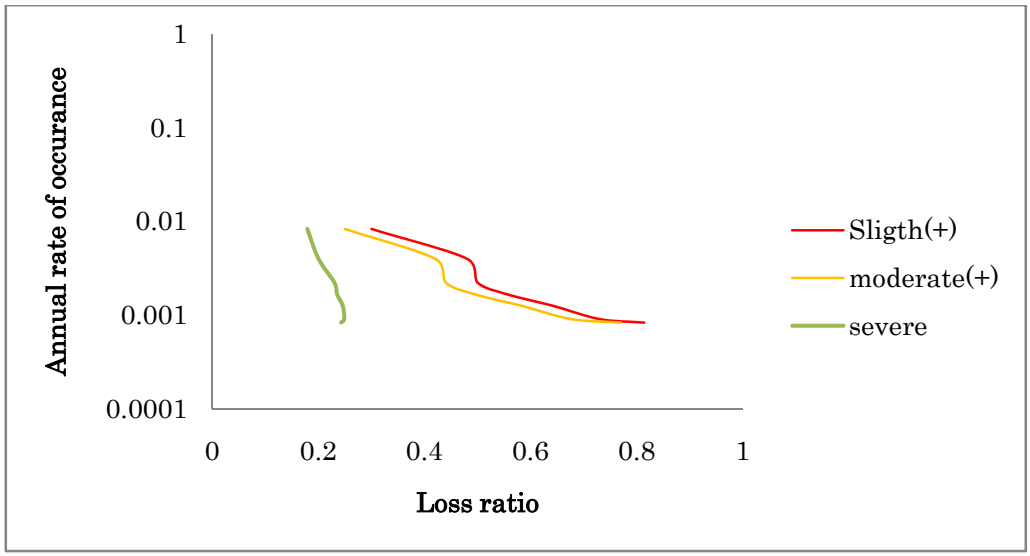


**Fig.20** Loss probability for each annual rate of occurrences.

## 5. CONCLUSIONS

According to microtremor array observations, downtown Padang is underlain by soft soil conditions ($V_{s30}$<400 m/s). Consistent results concerning the soil condition were found based on predominant period observations and the questionnaire survey. In both cases, the coastal area was determined to have a soft soil conditions ($V_{s30}$<400 m/s), a longer predominant period, and a greater seismic intensity.

These results provide critical information for making shaking maps, updating hazard maps, and developing disaster prevention countermeasures in Padang.

## REFERENCES

Aki, K. 1957. Space and time spectra of stationary stochastic waves, with special reference to microtremor, Bull. Earth. Res. Inst., Vol. 35, No. 3, 415-456.

Baker, Jack W. 2008. Introduction Probabilistic Hazard Analysis, handbook. Version 1.3 Oct 1st 2008.

BNPB 2009. Total damage report and verification for West Sumatra due to Padang earthquake.

Danny HilamNatawidjaja and WahyuTriyoso 2007. The Sumatran fault Zone-from Source to Hazard, J. of Earthquake and Tsunami, Vol. 1 No. 1, 21-47.

EERI 2009. The $M_w$ 7.6 Western Sumatra Earthquake of September 30, 2009, Special report.

Fauzi.(1999), Private home page available at www.gretchen.geo.rpi.edu/fauzi/xt).

Hamzah and Puspito. 2000. Tsunami Catalog and zones in Indonesia, J. of natural disaster

science, Volume 22, number 1, 2000, pp25-43.
Haskell, N.A. (1953), The dispersion of surface waves on multi-layered media, Bull. Of the Seismological Society of America, Vol.43, No.1, pp.17-24
Keneddy, J. and Eberhart, R. C. (1995), Particle swarm optimization, Proc. Of IEEE International conference on Neural Networks, Vol.4,pp.1942-1948
Mark D. Peterson et al. 2004. Probabilistic Seismic Hazard Analysis For Sumatera, Indonesia and Across the Southern Malaysian Peninsula Tectonophsysics 390 (2004) 141-158.
Ono, Y., Kiyono, J., Rusnardi, P. R. and Noguchi, T. 2010. Microtremor observation in Padang city, Indonesia to estimate site amplification of seismic ground motion, Proc. of International Symposium on a Robust and Resilient Society against Natural Hazards and Environmental Disasters and the third AUN/SEED-Net Regional Conference on Geodisaster Mitigation, pp.386-391.
Otha, Y., and Omote, S., (1977). An investigation into human psychology and behavior during an earthquake, proceeding of the 6th world conference on earthquake engineering 2, 499-504
Pemerintah kota Padang local government of Padang city). Available at at www.Padang.go.id (Padang local government website).
Prawirodirjo, L., Y. Bock, J.F. 2000, One century of tectonic deformation along the Sumatran fault from triangulation and global positioning system surveys, J. of Geophysical research, 105, 28, 343-28,363.
Rusnardi Rahmat Putra, J. Kiyono, Y. Ono. 2010, Seismic Hazard Analysis for Indonesia, Proc. of International Symposium on a Robust and Resilient Society against Natural Hazards and Environmental Disasters and the third AUN/SEED-Net Regional Conference on Geodisaster Mitigation, pp.317-325.
Rusnardi Rahmat Putra, J. Kiyono, Y. Ono, H Parajuli, Seismic Hazard Analysis For Indonesia. Journal of Natural Disaster Science, Vol. 33, No.3 pp.59-70, June 2012.
Rusnardi Rahmat Putra**,** J. Kiyono, Y. Ono, Estimation of Earthquake Ground Motion in Padang City, Indonesia. International Journal of GEOMATE, Vol..1 (S1.No.1), pp.71-77, October, 2011
Utsu, T. et al. 1992, Catalog of Destructive Earthquake in the world 1500-1992, in the Disaster Reduction handbook, International Institute of seismology and earthquake Engineering, Tsukuba Japan, I-24.